Radiative Heat Transfer in Self-Shielding Vapor Layer During Tokamak Disruptions

R.R. Peterson

August 1983

UWFDM-537

FUSION TECHNOLOGY INSTITUTE

UNIVERSITY OF WISCONSIN

MADISON WISCONSIN

Radiative Heat Transfer in Self-Shielding Vapor Layer During Tokamak Disruptions

R.R. Peterson

Fusion Technology Institute
University of Wisconsin
1500 Engineering Drive
Madison, WI 53706

http://fti.neep.wisc.edu

August 1983

UWFDM-537

RADIATIVE HEAT TRANSFER IN SELF-SHIELDING VAPOR LAYER DURING TOKAMAK DISRUPTIONS

R.R. Peterson

Fusion Engineering Program
Nuclear Engineering Department
University of Wisconsin-Madison
Madison, Wisconsin 53706

August 1983

UWFDM-537

I. Introduction

Plasma disruptions have been long known to be able to deposit large amounts of heat on the walls or limiters of tokamaks. It is anticipated that this plasma energy deposition could lead to melting, evaporation and large thermal stresses in the tokamak first surfaces. Any of these effects could severely limit the lifetime of the energy absorbing surface in a tokamak reactor, such as INTOR.[1] Previous studies have addressed the problems of evaporation and melting[2-5] and have provided some estimates of first wall erosion rates. Thermal stresses and plastic deformation of the first wall have been found to be severe even for the cases where no melting or vaporization of the first wall occurs.[6] The stability of the melt layer under the influence of the force generated by the eddy currents in the material and the magnetic fields has been addressed and it has been determined that the reactor can be designed so that layer is stable.[7]

In some of these studies, it has been found that when vaporization of the metal in the first wall occurs that some of the energy of the disruption is absorbed in this vapor.[2,5] Hassanein assumed that one-half of the energy by this vapor is radiated to the wall and found some significant reductions in the first wall melting and vaporization. Thus, the concept of the self-shielding vapor layer may be important to tokamak first wall design and should be analyzed in more detail. The opacity of the vapor may be high enough that the radiation transport is non-isotropic. The variation of the density profile of the vapor in time and space will lead to a complicated transport of the energy in the vapor. In this article, calculations are presented of radiative heat transfer in this self-shielding vapor.

The radiative heat transfer in the self-shielding vapor is depicted in Fig. 1. The first frame shows disruption ions streaming towards the tokamak wall. Vaporization then occurs and the vapor moves into the plasma. Eventually, enough vapor accumulates to absorb appreciable amounts of ion energy. This energy deposition creates a hot region in the vapor which radiates some of that deposited energy away. The questions addressed in this study are where does this radiation go and how rapidly is the deposited energy radiated away.

II. Computational Method

To calculate the radiative heat transfer in the self-shielding vapor, a simulation computer code developed at the University of Wisconsin has been used. This code, called FIRE, is a Lagrangian radiation transport hydrodynamics code which has been used previously mainly for inertial confinement fusion applications.[8] In the mode used for these calculations, the vapor and the radiation are modeled as two "fluids," each with its own temperature. The radiation "fluid" has a temperature which is proportional to the fourth root of the energy density of the radiation field. The radiation fluid is allowed to move through the vapor as predicted by a diffusion model where the radiation conductivity is related to the Rosseland opacity[9] through

$$K_R = 10^{10}/\rho\sigma_R \qquad (cm^2/sec) \qquad (1)$$

where ρ is the vapor density in g/cm^3 and σ_R is the Rosseland opacity in cm^2/g. An upper limit is placed on the radiation conductivity so that, in cases where the Rosseland opacity is very small, radiation will not diffuse faster than the speed of light. Absorption and emission of radiation by the

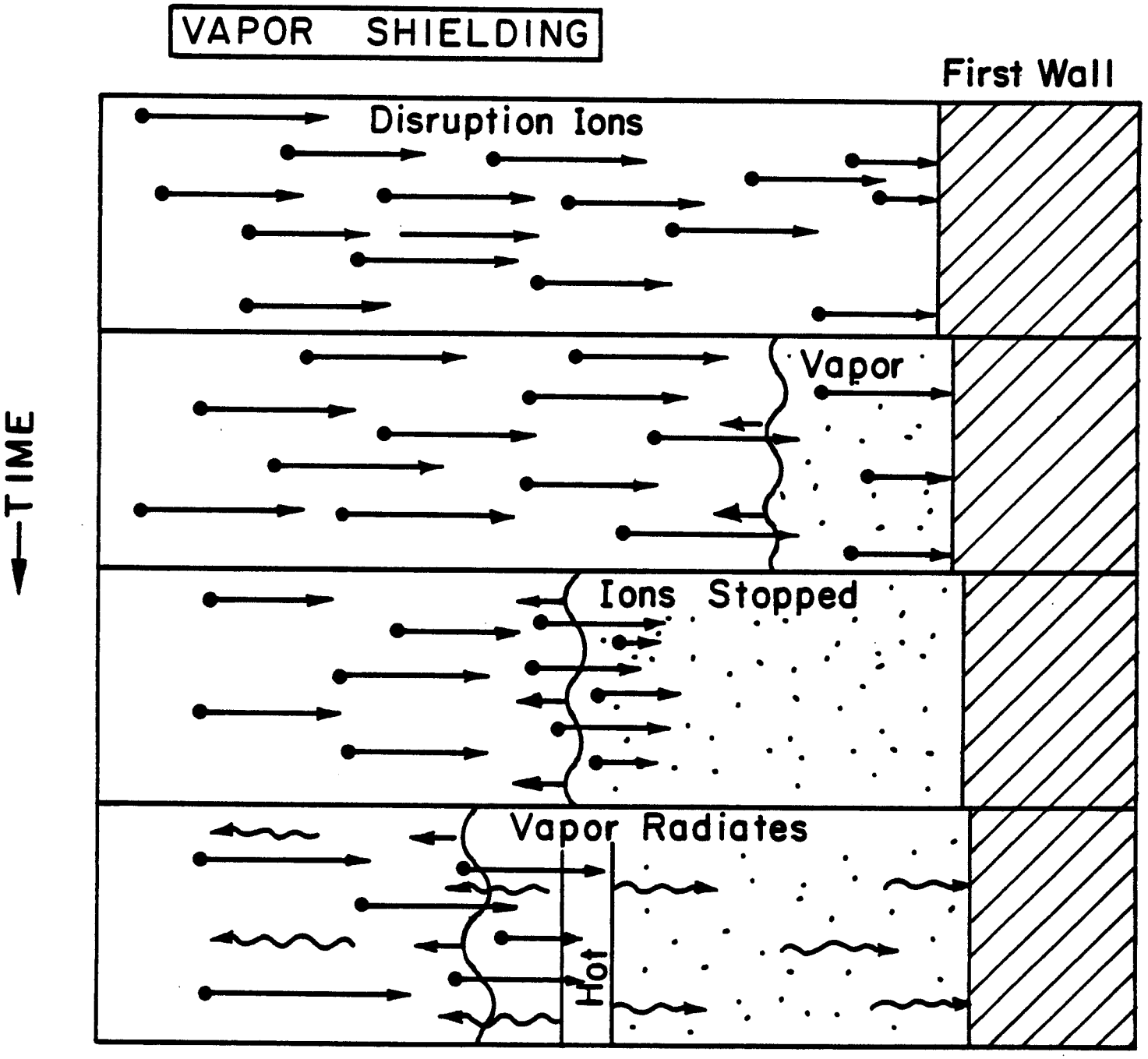

Fig. 1. Schematic picture of radiation transport in self-shielding vapor.

vapor is modeled with an energy exchange term between the two fluids. The rate of energy flow to the vapor from the radiation is written as

$$\Delta E_{exchange} = \omega_R E_R - \omega_P E_P \ , \tag{2}$$

where E_R is the radiation energy density and E_P is the energy density of the vapor. The plasma absorption coefficient is

$$\omega_R = c\sigma_p \tag{3}$$

and the emission coefficient is

$$\omega_P = 4\ T_P^3 \sigma_P \ , \tag{4}$$

where T_P is the local temperature of the vapor and c is the speed of light. σ_P is the Planck opacity.[9]

The equation of state of the vapor as well as the opacities can greatly affect radiative heat transfer in the vapor. For this reason, equations of state and opacities must be obtained for the vapor at the relevant densities and gas temperatures. A computer code has been developed at the University of Wisconsin, called MIXERG,[10] which calculates these quantities and provides them in a form readable by FIRE. In Fig. 2, the internal energy density of vaporized 316 stainless steel (12% Ni, 17% Cr, 2.0% Mo, 0.004% C, 0.5% Si) is plotted against gas temperature and density. There are sharp rises in the internal energy density at the combinations of vapor temperature and density at which ionization occurs. The ionization of the vapor is calculated in the

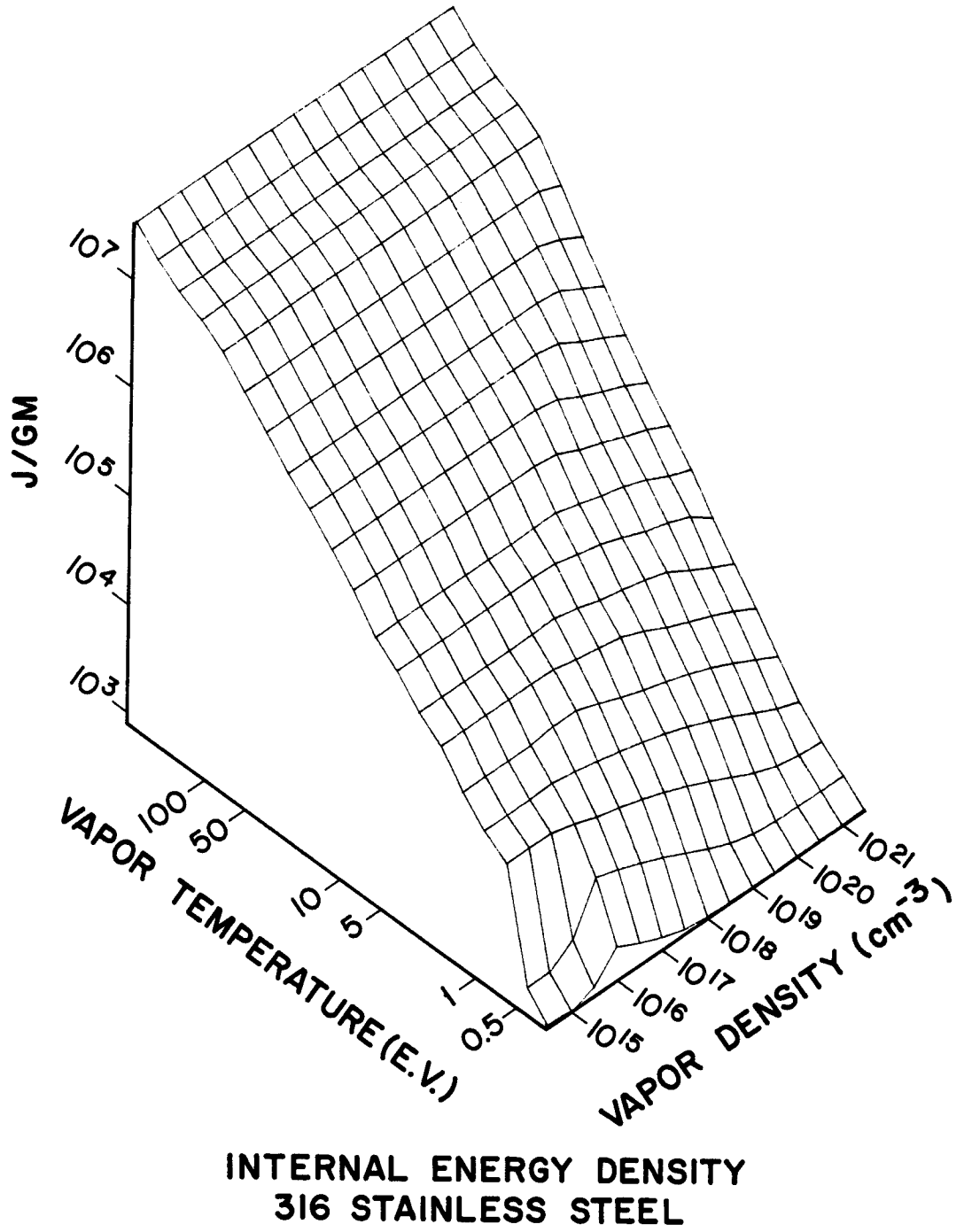

Fig. 2. Internal energy density of vaporized 316 stainless steel versus vapor temperature and density.

Saha or Coronal model,[11] depending on what vapor density and temperature are considered. The Rosseland opacity for 316 stainless steel is shown in Fig. 3, where it is plotted against the vapor and radiation temperatures for a Fe vapor density of 2.7×10^{19} cm^{-3}. This plot shows that at low plasma temperature and low radiation temperature the opacity drops in value. The general decrease in opacity at high radiation temperature, which occurs because of the ν^{-3} dependence on the photoionization cross section, may also be seen. The Planck opacity has a similar behavior.

III. Model for Disruption Vapor

The simulation computer code FIRE described in the previous section cannot model the vaporization of steel off of the tokamak first wall because the flow is not purely hydrodynamic. Thus, the density profile of the vapor at the start of the FIRE run must be provided to the code. Indeed, it is assumed that the heat transfer processes of interest occur more rapidly than does the motion of the vapor and the density profile of the vapor is taken to remain constant during the simulation. An analytic model for this density profile of the vapor at the start of the simulation is discussed in this section.

Assuming that the speeds of the vapor particles leaving the surface are distributed in a Maxwellian with temperature T_S (the surface temperature of the wall), the time derivative of the distribution function at time t' of these particles is

$$\dot{F}(v_z,t') = n_{SOLID} V_S(t') \left(\frac{m}{2\pi k_B T_S}\right)^{1/2} \exp\left[-\frac{v_z^2 m}{2k_B T_S}\right] . \qquad (5)$$

Here, V_S is the speed at which the solid or liquid surface is moving into the

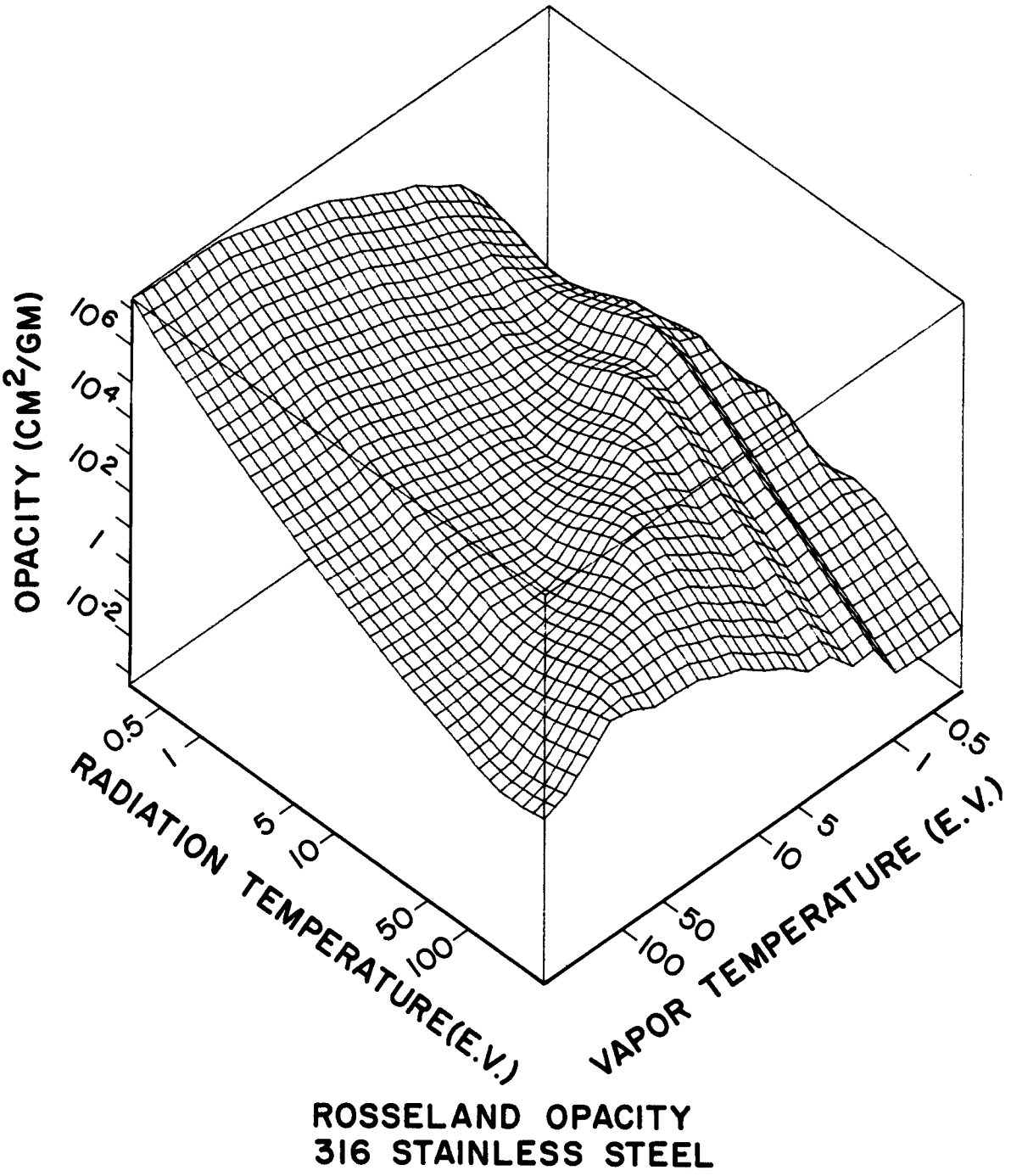

Fig. 3. Rosseland opacity for vaporized stainless steel for a Fe vapor density of 2.7×10^{19} cm^{-3} versus blackbody radiation temperature and vapor temperature for two vapor temperatures.

wall, n_{SOLID} is the particle density of the wall when it is a solid and m is the average mass of a vapor ion. This expression represents the rate at which vapor atoms are released from the surface at a given time and at a given velocity. One can determine the rate that atoms leaving the surface will populate the space between z and z + Δz from the surface of the wall at time t if one assumes that the atoms move independently of each other by integrating in v_z from $z/(t - t')$ to $(z + \Delta z)/(t - t')$. Dividing by Δz and taking the limit as Δz approaches 0 gives the time rate of change of particle density at time t at z due to evaporation at time t':

$$\dot{n}(z;t,t') = \frac{1}{(t - t')} \dot{F}\left(\frac{z}{t - t'}, t'\right) . \tag{6}$$

If V_S and T_S are assumed to be independent of time, one can integrate Eq. (6) with respect to t' and make appropriate changes in variables to obtain an analytic expression for the vapor density profile at time t:

$$n(z,t) = n_{SOLID} V_S \left(\frac{m}{2\pi k_B T_S}\right)^{1/2} E_1\left(\frac{z^2 m}{2k_B T_s t^2}\right) , \tag{7}$$

where E_1 is the exponential integral,

$$E_1(z) = \int_z^\infty dz \, \frac{e^{-x}}{x} .$$

This density profile at a few times after the start of the disruption is plotted in Fig. 4. T_S has been taken as 2700°K and V_S has been taken as 0.11 cm/sec; both numbers are consistent with Hassanein's calculations for a 650 J/cm^2, 10 msec disruption where 1/2 of the ion energy absorbed by the vapor is

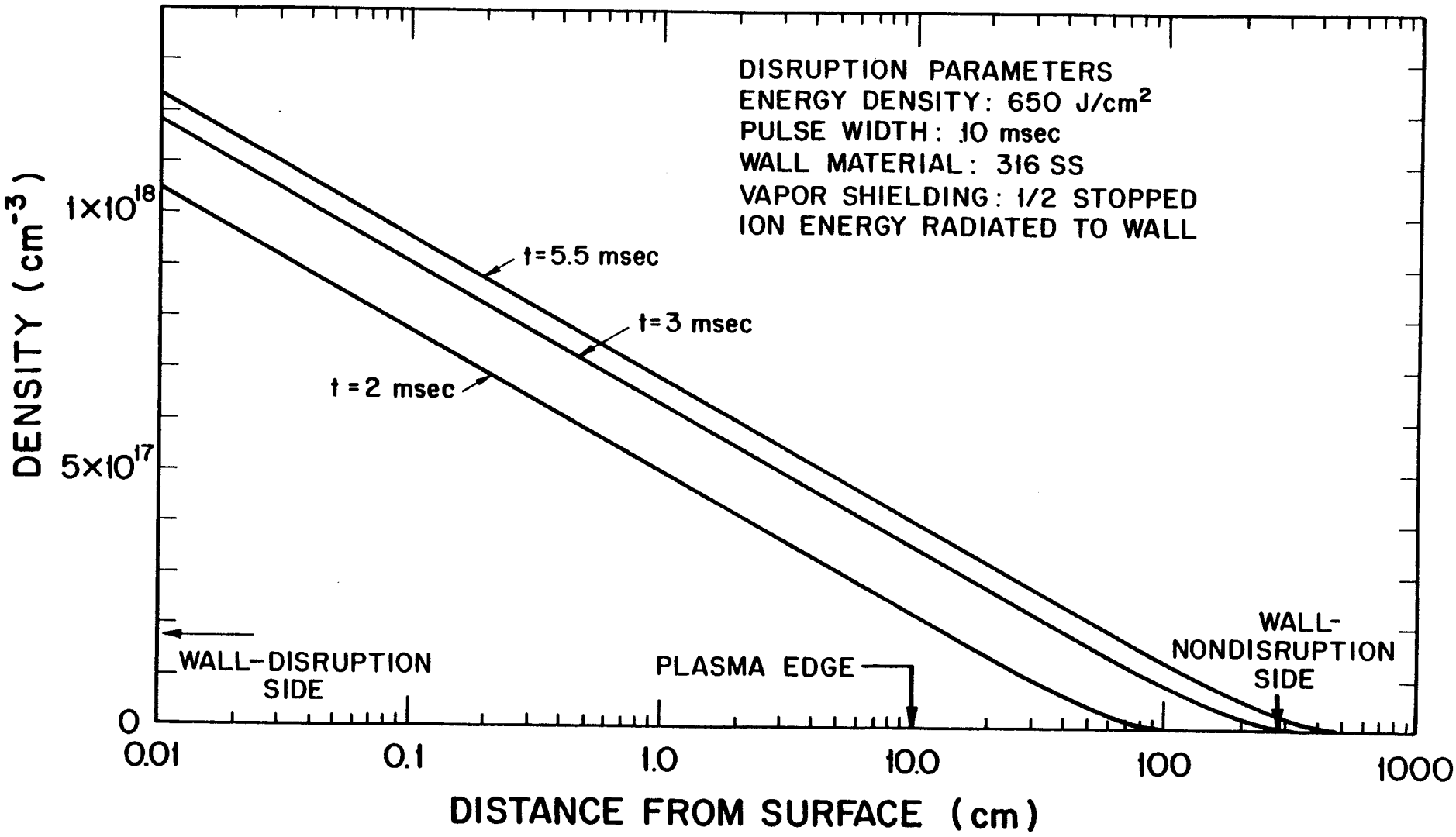

Fig. 4. Vapor density resulting from a self-shielding 650 J/cm^2 disruption with a 10 msec duration shown at a few times after the start of the disruption.

assumed radiated to the wall.[2] The mass of the average steel ion is 9.29 x 10^{-23} gm and the solid density is 8.5 x 10^{22} atoms/cm^3. Also shown in Fig. 4 are the position of the edge of the plasma nearest the vaporizing wall and the position of the wall on the opposite side of the vacuum vessel consistent with a tokamak which could experience a 650 J/cm^2 disruption.[1]

The rate that material is vaporized off of the wall is governed by the parameter V_S, which is chosen through a set of assumptions and some extrapolations from other work. Figure 5 shows the thickness of the evaporated layer due to 1000 disruptions on a stainless steel wall as calculated by Hassanein.[3] This thickness is plotted against disruption energy fluence in J/cm^2 for a few disruption durations and for cases where no vapor shielding is assumed as well as for cases where the vapor protects the wall from half of the disruption energy which it absorbs. From this figure, one can see that for 650 J/cm^2 of disruption energy over a 10 msec pulse width where vapor shielding is allowed that 10^{-3} cm of material is evaporated by each disruption. Notice that for the same case but for no vapor shielding roughly 5 times as much material is vaporized. V_S is plotted against time for a few duration times under the assumption of no vapor shielding in Fig. 6 for a disruption energy of 650 J/cm^2. The postulated value of V_S for the case with vapor shielding has been added which is shown as the cross-hatched region in Fig. 6. Notice that the area of this cross-hatched region is 1/5 the area under the 10 msec curve such that it agrees with the results in Fig. 5. Thus, V_S = 0.11 cm/sec was used from 1 msec to 10 msec after the start of the disruption and V_S = 0 otherwise.

The temperature profile of the vapor is certainly important to the radiant heat transfer in the vapor. The most important factor in determining the

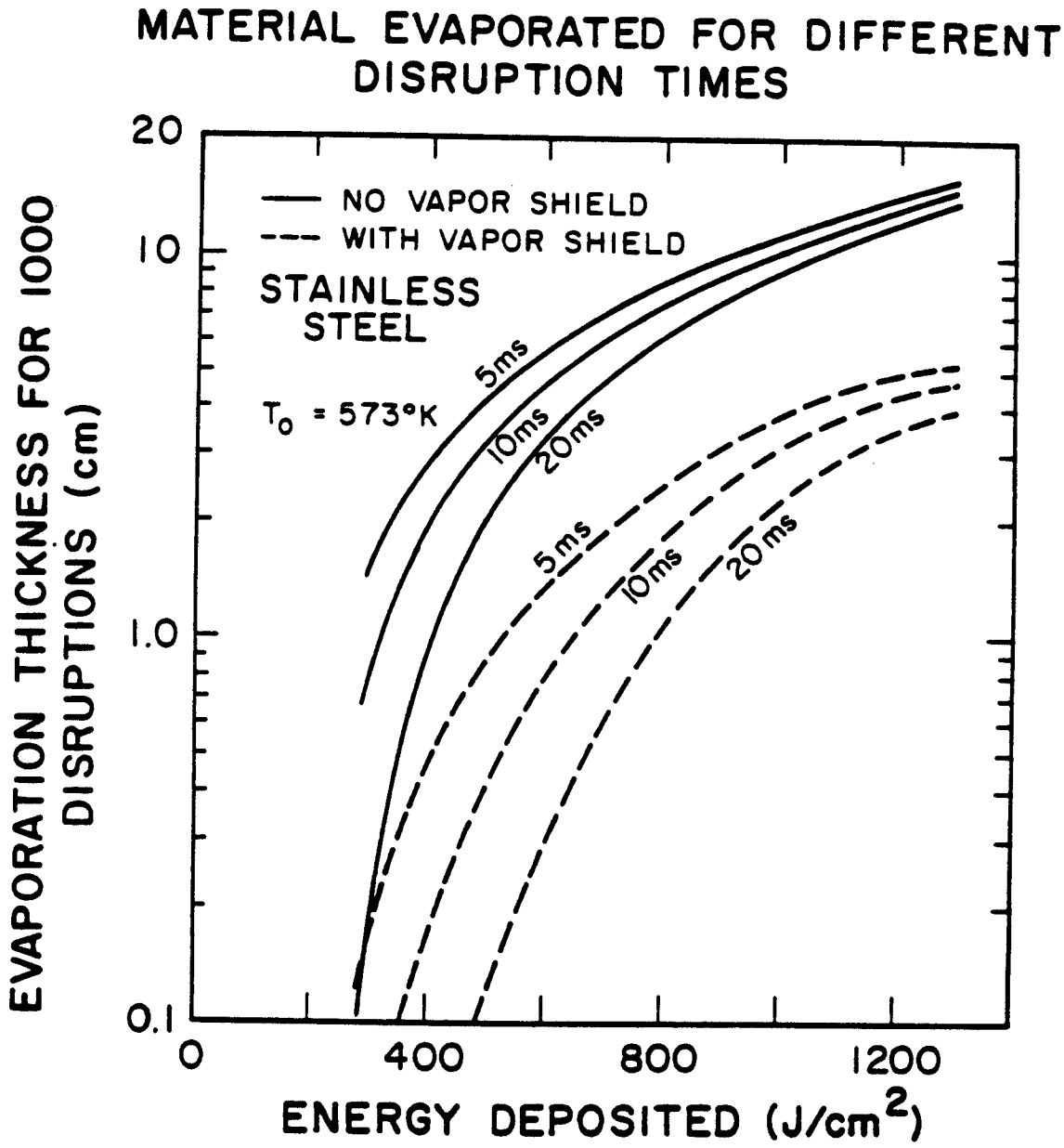

Fig. 5. Thickness of material evaporated off of a stainless steel wall by 1000 plasma disruptions both with and without self-shielding versus disruption energy fluence.

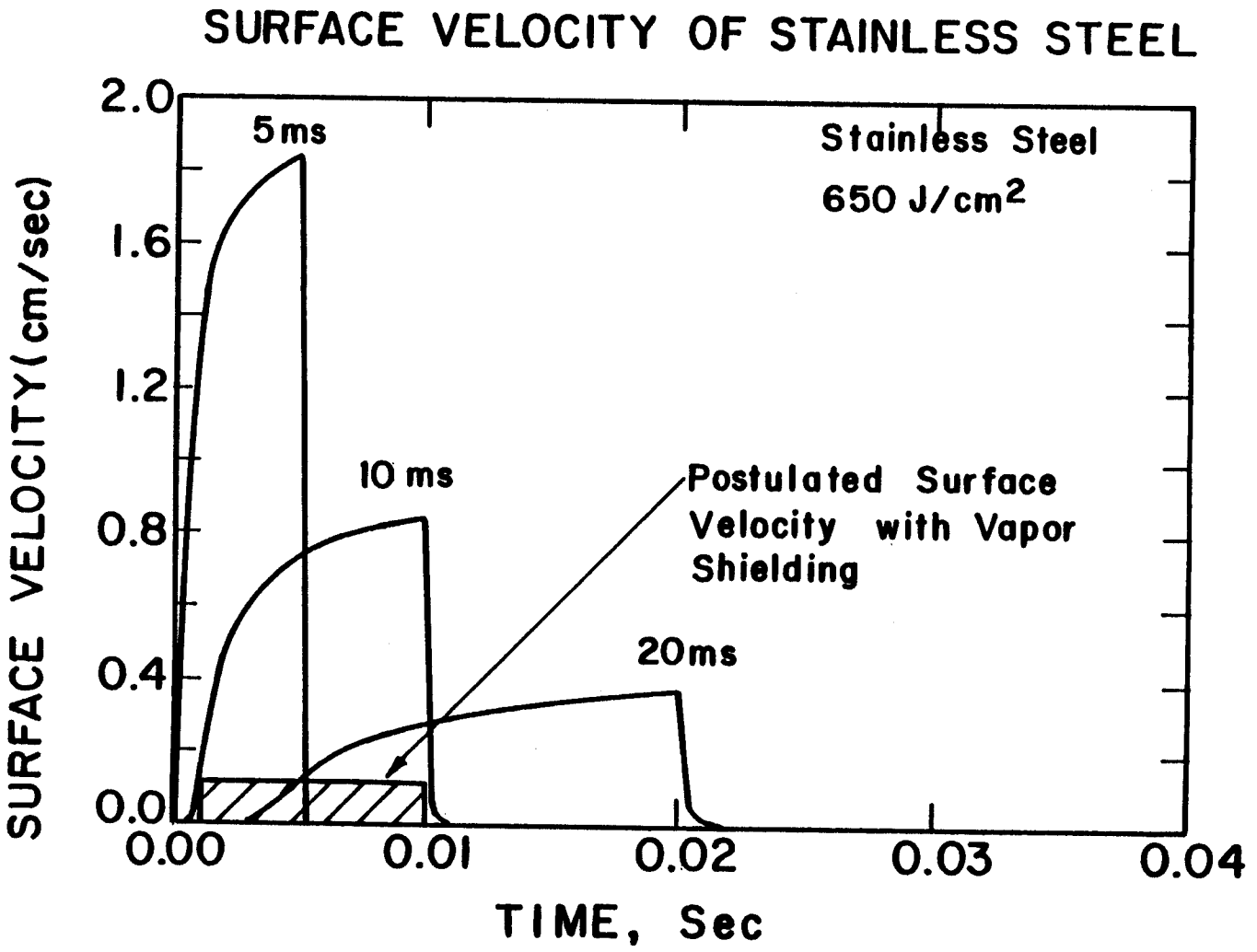

Fig. 6. The velocity at which the surface of the vaporizing stainless steel wall is eroded due to a 650 J/cm^2 disruption versus time. Velocities are shown for disruption durations of 5 msec, 10 msec and 20 msec for no self-shielding. Also shown is the velocity postulated for the case with self-shielding and a 10 msec disruption durations.

vapor temperature profile is the energy deposition profile of the disruption ions. It's assumed that the disruption ions are 20 keV D and T. The area/density for stopping these ions in steel is taken to be 5.93×10^{-5} g/cm^2 $\equiv \rho R_{stop}$. Furthermore, it's assumed that the energy deposition is exactly proportional to the particle density; that is,

$$\begin{aligned} \frac{1}{\rho}\frac{dE}{dr} &= C \ , \qquad \rho R \leq \rho R_{stop} \\ &= 0 \ , \qquad \rho R \ \& \ \rho R_{stop} \ , \end{aligned} \tag{8}$$

where E is the ion energy, r is the incremental length along the ion's trajectory and R is the length travelled by the ion through the vapor. The requirement that the ions enter the vapor with 20 keV of energy demands that C is 5.4×10^{-11} J-cm^2/g. Thus, the deposition profile begins at the edge of the plasma nearest the vaporizing wall and continues, proportional to the vapor density up to the point where the ions run out of energy. It is somewhat arbitrary that the ions only begin to deposit energy into the vapor at the point that was the edge of the plasma before the disruption. As the vapor moves into the center of the vacuum vessel it will absorb energy from the plasma ions. This process may be a topic for future study.

IV. Computational Results

The FIRE and MIXERG computer codes have been used to simulate radiant heat transfer in the vapor described in Section III. Simulations have been completed in vapor profiles 1 msec and 5.5 msec after the start of the disruption. The results of these two simulations are summarized in Table I.

Table I. Radiant Energy on Tokamak Walls Integrated over 0.1 msec

Time after start of disruption	1 msec	5.5 msec
Maximum heat flux on shielded wall	5.16 kW/cm^2	3.88 kW/cm^2
Maximum heat flux on unshielded wall	0.60 kW/cm^2	2.41 kW/cm^2
Radiant energy in 0.1 msec on shielded wall	0.64 J/cm^2	0.52 J/cm^2
Radiant energy in 0.1 msec on unshielded wall	0.01 J/cm^2	0.30 J/cm^2
Energy deposited by ions	6.56 J/cm^2	6.52 J/cm^2

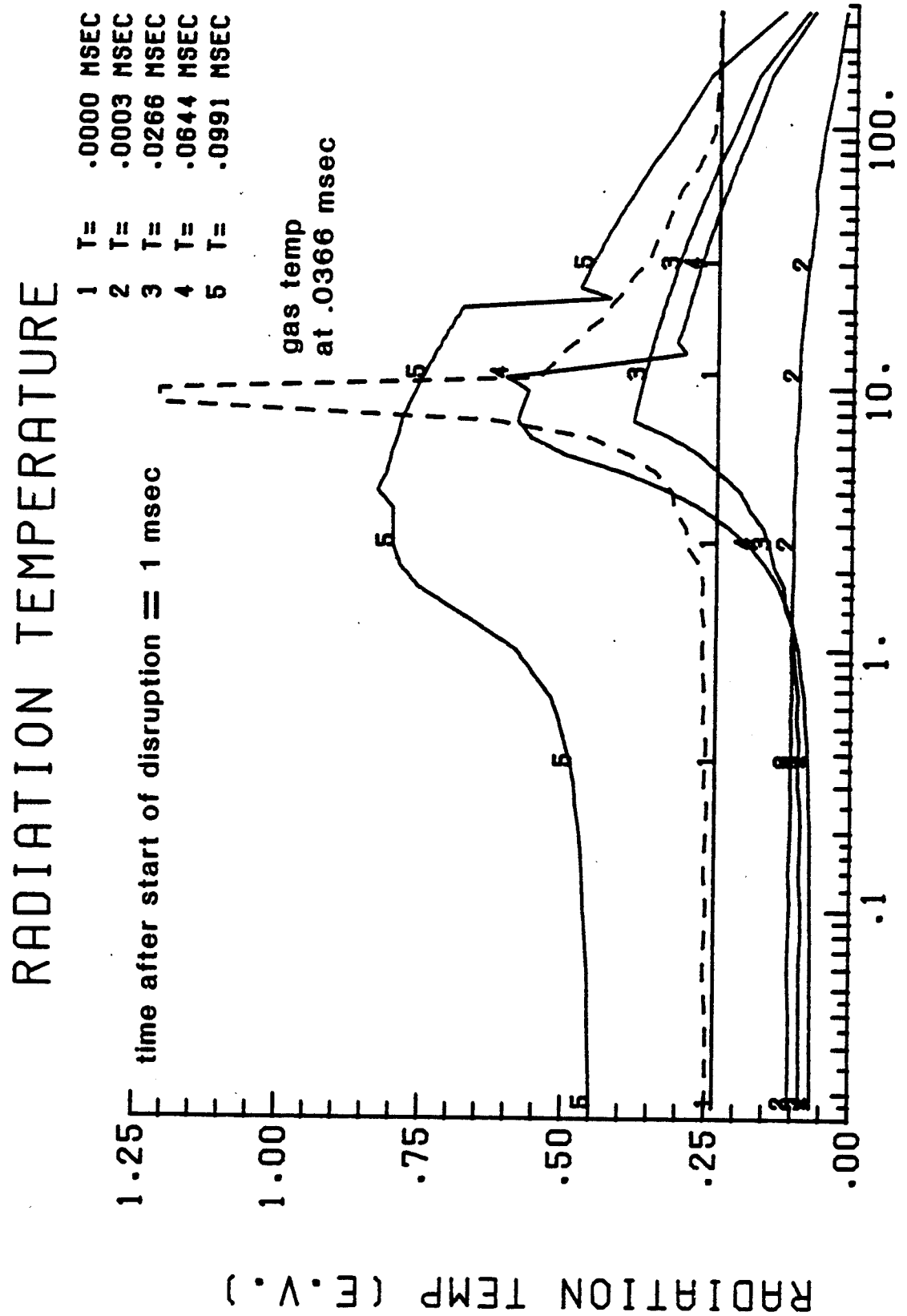

Fig. 7. Radiation temperature profiles plotted at several different times.

Simulation results for the density profile at 1 msec after the start of the disruption are shown in Figs. 7, 8 and 9. Figure 7 shows the temperature of the radiation plotted against distance from the vaporizing surface at several different times. The vapor temperature is also shown plotted at 1.0336 msec after the start of the disruption.

The calculation starts with a uniform temperature at 1 msec of 0.25 eV. The radiation temperature very quickly drops to 0.1 eV as the vapor begins to radiate. The Rosseland opacity is shown plotted against position in Fig. 8 for the same times as the radiation temperatures are plotted in Fig. 7. One can see that for early times the opacity is very low and that it is somewhat higher near the vaporizing wall. This explains why the radiation temperature quickly drops and why it is a little higher near the vaporizing wall.

As ions are continually being absorbed by the vapor within 10 cm of the vaporizing wall, the vapor heats up and the opacity of the vapor in this region increases drastically. There is always a more rapid drop-off in the opacity as one moves towards the vaporizing wall than as one moves towards the other wall. This means that, later in time, more radiation energy should reach the vaporizing wall. This is shown to be true in Fig. 7, where it can be seen that the radiation temperature drops to a low level before reaching the opposite wall. This is further clarified in Fig. 9 where the radiant heat fluxes on the vaporizing and non-vaporizing walls are plotted against time. Here it can be seen that the heat fluxes are initially very much the same in both directions but that after 1.001 msec there are pulses of radiant energy on the vaporizing wall which are much higher than those appearing on the non-vaporizing wall.

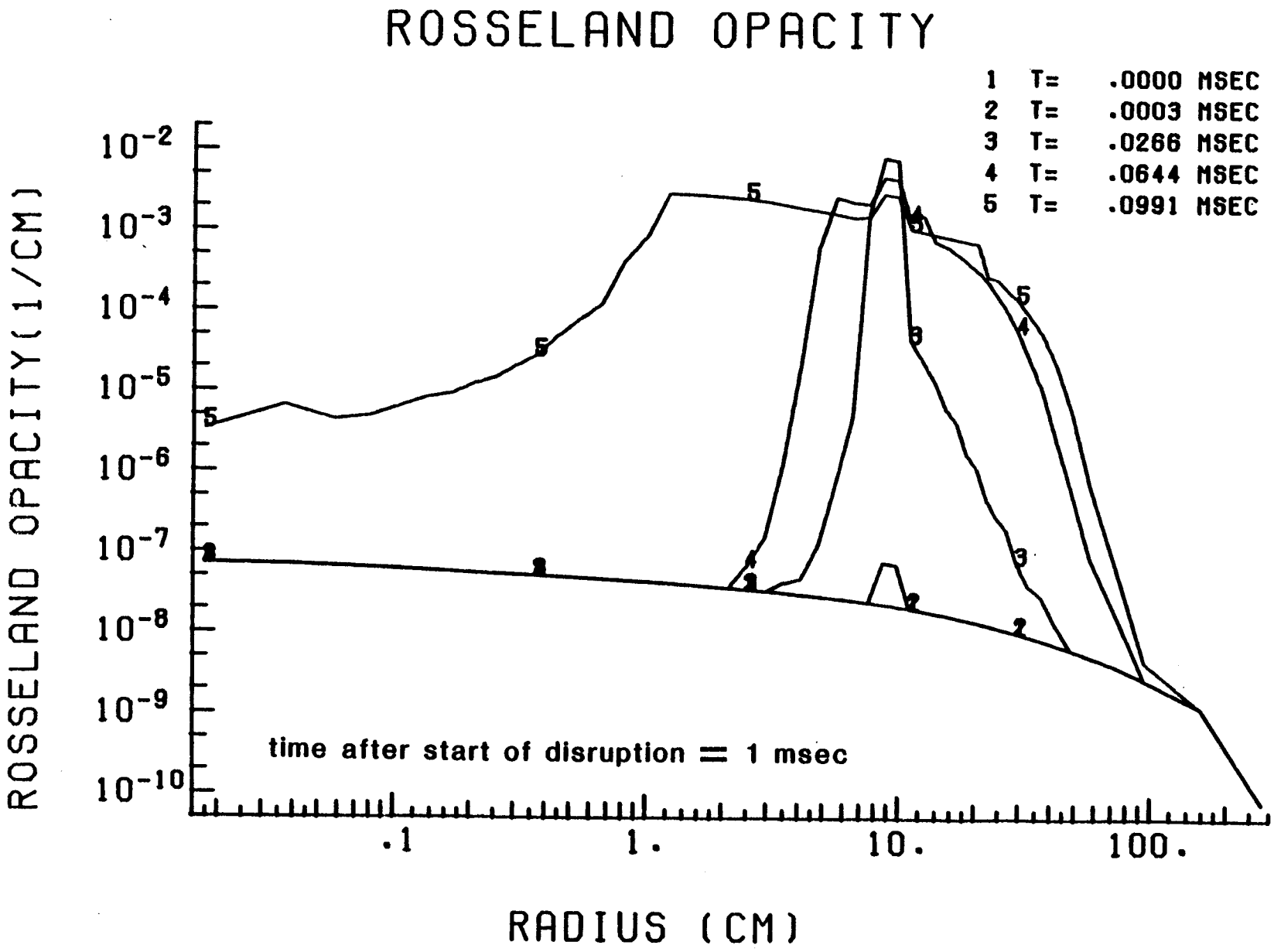

Fig. 8. Rosseland opacity profiles at the same times as in Fig. 7.

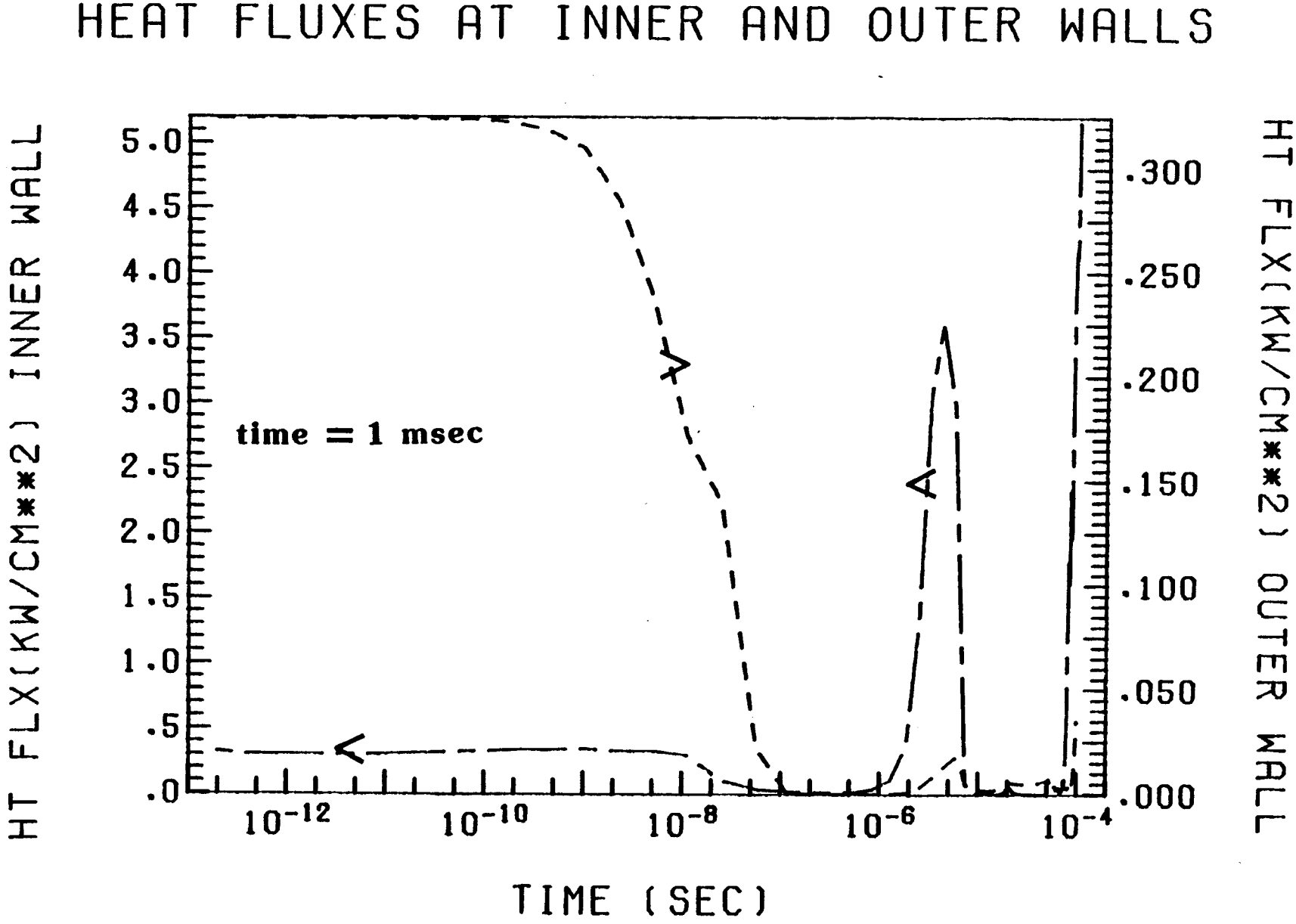

Fig. 9. Radiant heat fluxes on vaporizing and non-vaporizing wall versus time.

Similar results are shown in Fig. 10 for the vapor density profile present at 5.5 msec after the start of the disruption. Once again, the radiation heat fluxes are plotted against time and the radiation has been found to be initially roughly isotropic. As in the case of the vapor density profile at 1 msec after the start of the disruption, later in time the vaporizing wall sees a higher heat flux than does the other wall.

These results are summarized in Table I. In both cases approximately 6.5 J/cm^2 are deposited into the vapor by ions during the calculation. In the case 1 msec after the start of the disruption, the unshielded wall (that wall opposite to the vaporizing wall) sees a maximum heat flux one-tenth of that seen by the vaporizing wall. The difference is not nearly so large 5.5 msec after the start of the disruption. A similar statement can be made about the radiant energy in 0.1 msec where the anisotropy is much larger 1 msec than 5.5 msec after the start of the disruption. The degree of anisotropy in the radiation transfer is due to the opacity profile in the vapor. It is not surprising that the opacity profiles are different 5.5 msec after the start of the disruption than 1 msec after, though the details of why the radiation transfer is more isotropic at 5.5 msec are not known at this time.

V. Discussion and Conclusions

The results of computer simulation indicated that radiation transport in the wall material vaporized during a tokamak disruption is not necessarily isotropic. This is due to the strong temperature dependence of the vapor to thermal photons. Therefore, the temperature profiles, induced by the deposition of disruption ions in the vapor, can cause opacities which vary greatly over small distances. Radiation will propagate in the directions where the opacities are low so the propagation can be very non-isotropic.

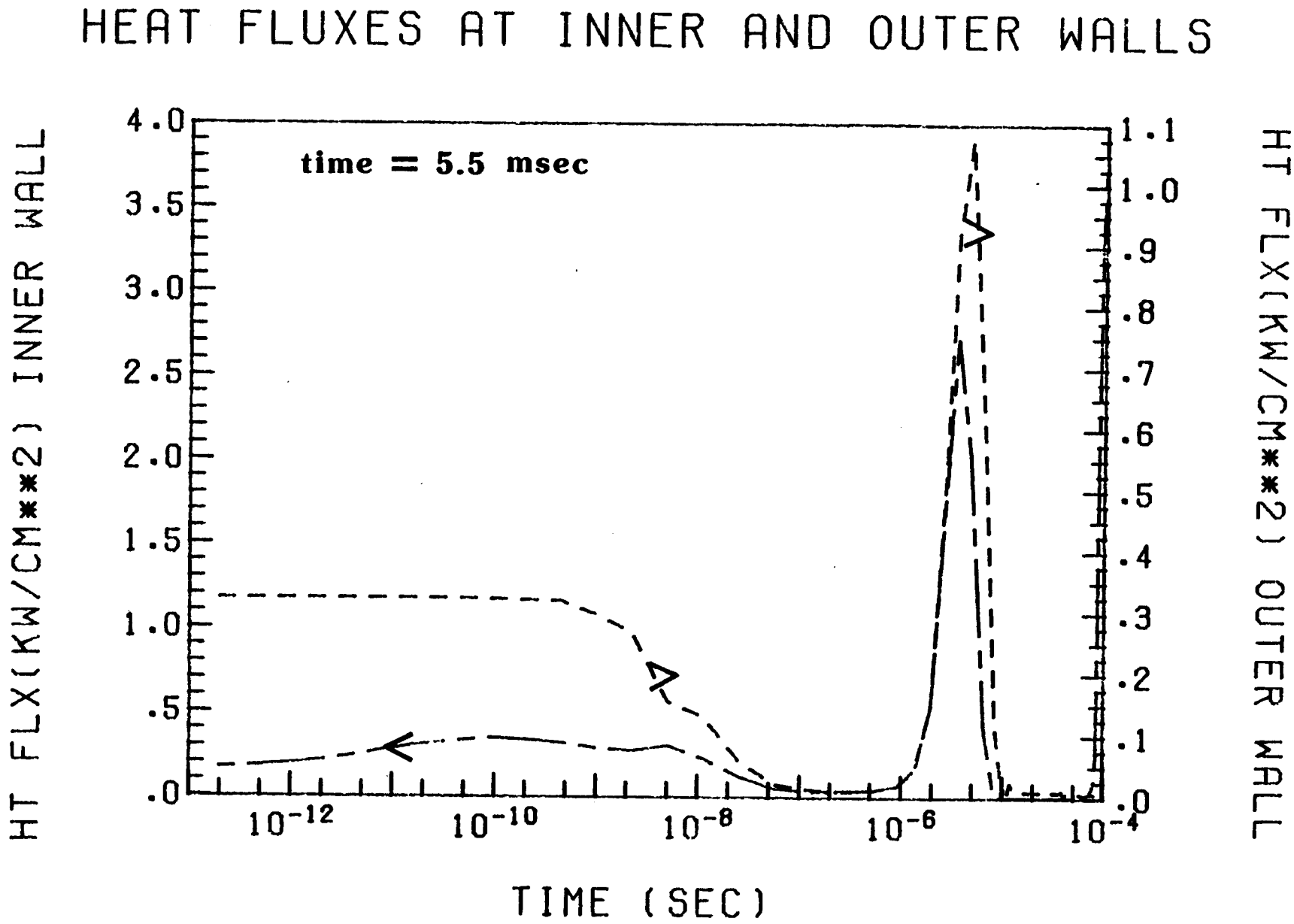

Fig. 10 Radiant heat fluxes on vaporizing and non-vaporizing wall versus time.

In addition to the non-isotropic nature of the radiative heat transfer, a computer simulation has established that most of the energy deposited by the disruption ions is radiated away by the vapor within 10 msec. This is shown in Table II where the energy deposited by the ions, the energy radiated to the unshielded and shielded walls in 10 msec are given for the density profile of 1 msec after the start of the disruption. The neglect of the hydrodynamic motion of the vapor is of course not valid when the simulation takes place over 10 msec. The vapor will move about and the total mass of vapor will increase greatly over 10 msec. However, since this simulation shows that 98% of the ion energy is radiated away, one might suggest that, even if the mass of vapor has greatly increased by 11 msec, the majority of the ion energy is still radiated away quickly.

These two general results lead to the conclusions that radiation from the vapor is the major means by which ions late in the disruption may contribute to vaporization of the wall and that the nature of this radiative heat transfer should be considered carefully. The simulations presented here are not sophisticated enough to make a definitive statement about the effectiveness of self-shielding by the vapor. The results in Table I show that radiant energy densities are higher on the shielded wall than on the unshielded wall, an effect which would become even more pronounced if multi-dimensional geometrical effects were considered. However, changes in the density profiles due to the increased vaporization might increase the self-shielding effect. Another effect which has been neglected is initial non-uniform temperature profiles in the vapor. Simulations have been made over 0.1 msec where the initial temperature profile is uniform. Once simulations can be done over 10 msec, the very

Table II. Radiant Power Density on Tokamak Walls Integrated to 10 msec

Time after start of disruption	1 msec
Radiant energy in 10 msec on shielded wall	636 J/cm^2
Radiant energy in 10 msec on unshielded wall	1.53 J/cm^2
Energy deposited by ions	651 J/cm^2

non-uniform temperature profile may lead to very different results from those shown in Table I.

Several improvements to the simulation code should be made before the effectiveness of the self-shielding vapor can be determined. The most important improvement would be self-consistent calculation of the vaporization and the radiative heat transfer. Another improvement would be addressing the possible dilution of the plasma by the vapor which could reduce the energy in ions. These improvements are currently under development.

Acknowledgment

Support for this work provided by U.S. Department of Energy under contract DE-AC02-82ER52082.

References

1. "INTOR - U.S. Contribution to the International Tokamak Reactor Phase-I Workshop," USA INTOR/80-1 (June 1980).

2. A.M. Hassanein, G.L. Kulcinski and W.G. Wolfer, J. Nucl. Mater. 103/104, 321 (1981); J. Nucl. Mater. 111/112, 554-559 (1982).

3. B.J. Merrill, Proc. 9th Symp. on Engineering Problems of Fusion Research, Chicago, IL (1981), p. 1621.

4. J.A. Fillo and H. Makowitz, Proc. 9th Symp. on Engineering Problems of Fusion Research, Chicago, IL (1981), p. 1775.

5. B.J. Merrill and J.L. Jones, J. Nucl. Mater. 111/112, 544-547 (1982).

6. R.R. Peterson and W.G. Wolfer, J. Nucl. Mater. 111/112, 541-543 (1982).

7. W.G. Wolfer and A.M. Hassanein, J. Nucl. Mater. 111/112, 560-565 (1982).

8. T.J. McCarville, R.R. Peterson and G.A. Moses, "Improvements in the FIRE Code for Simulating the Response of a Cavity Gas to Inertial Confinement Fusion Target Explosions," Computer Physics Communications 28, 367-403 (1983).

9. D. Mihalas, Stellar Atmospheres, W.H. Freeman and Co., San Francisco, (1978).

10. R.R. Peterson and G.A. Moses, "MIXERG - An Equation of State and Opacity Computer Code," Computer Physics Communications 28, 405-426 (1983).

11. D. Mosher, "The Coronal Equilibrium of High Atomic Number Plasmas," NRL Memorandum Report 2563, Naval Research Laboratory (March 1973).